Effects of Waveguide Wall Grooves Used to Hold Samples for Measurement of Permittivity and Permeability

Raymond Luebbers, *Senior Member, IEEE*

Abstract— **The complex permittivity and permeability of a material may be measured at microwave frequencies by placing a sample of the material in a waveguide and measuring the complex reflection and transmission coefficients. Whereas there are various approaches to holding the sample in place, for a thin rigid sample shallow grooves may be cut in the waveguide walls for this purpose. However, such grooves will be a source of error since higher order modes can be excited. In this paper the modal analysis method is used to illustrate the potential for error in measuring constitutive parameters of the sample introduced by the grooves.**

I. Introduction

THE complex permittivity and permeability of a material at microwave frequencies may be determined by placing a sample in a waveguide and measuring the complex reflection and transmission coefficients. If the sample exactly fits the waveguide cross section and has planar ends perpendicular to the waveguide axis, the necessary calculations are straightforward applications of transmission line methods, since (assuming single mode propagation in the air-filled section of waveguide) only a single mode propagates throughout the measurement volume. Even if the constitutive parameters of the material are large enough so that higher order modes may propagate within the material sample, they will not be excited.

In reality such a situation as described here will not exist exactly. One source of error is air gaps, where the material sample does not exactly fit the waveguide walls. This error source has been investigated in [1] using the modal analysis method of Wexler [2]. In [1] the conclusion was that errors due to small air gaps could essentially be eliminated by using a conducting paste to fill the gaps.

A more difficult error source to remove is encountered when a thin material sample, much thinner than the transverse dimensions of the waveguide, must be held in the waveguide. This situation occurs when measuring the complex permittivity and permeability for very thin, anisotropic material samples at low frequencies. The anisotropy prevents the use of coaxial measurement fixtures, and free space measurements may not have sufficient accuracy. Since very large waveguides must be used, the sample thicknesses are only a small fraction of the waveguide transverse dimensions, and typical sample holders cannot reliably hold the samples perpendicular to the waveguide axis.

Manuscript received December 18, 1990; revised July 20, 1991, and February 9, 1993. This work was supported in part by Lockheed Missiles & Space Co., Sunnyvale, CA.

The author is with the Department of Electrical and Computer Engineering, The Pennsylvania State University, University Park, PA 16802.

IEEE Log Number 9212729.

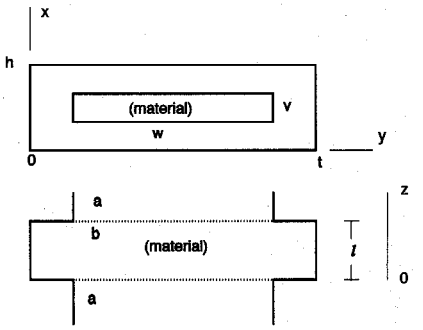

Fig. 1. Waveguide with material sample in the groove.

One approach to holding thin rigid slabs of material perpendicular to the measurement waveguide axis is to cut a small groove in the waveguide walls the same thickness as the sample and just deep enough to hold it in place, as in Fig. 1. In reality, this groove would be part of a waveguide mechanical junction, but for analysis purposes we can neglect this complication.

The sample is in region b and is of thickness ℓ. The sample is assumed to fill exactly the dimensions of waveguide b, which is larger than waveguide a. Not shown in Fig. 1 are the locations of the waveguide probes used to sample the reflected and transmitted fields to determine the complex reflection and transmission coefficients and thus the complex constitutive parameters of the sample.

The inclusion of the waveguide groove (which forms waveguide b) to hold the sample introduces errors in the measurements. These errors are due to the excitation of higher order modes in the sample material and in the external "a" waveguides. These higher order modes have several unwanted effects. First, the determination of the complex constitutive parameters of the material assumes single mode propagation through the waveguide system. If higher order modes can propagate in waveguide section b, they may now be excited by the grooves at the intersection of waveguides a and b. Second, the reflection and transmission coefficients will be changed due to the presence of fringing fields at the waveguide junctions.

To provide a means of determining the error introduced in the measurement due to the presence of the groove, a

modal analysis [2] of the sample holding geometry has been performed. The details of the method are contained in [2] and [3], and are summarized in later sections of this paper. The convergence of the modal solution as the number of modes in each waveguide section is increased is also demonstrated.

Once the modal coefficients are determined, the fields at any location in the waveguide system can then be found. The modal analysis is completely general in that the waveguide dimensions w, v, t, h, the sample thickness ℓ, the complex constitutive parameters of the sample, and the locations where the reflected and transmitted fields are sampled, may be specified arbitrarily. The sample may be anisotropic provided that the tensors are diagonal and with the x and z components of both tensors equal to each other. In addition, to simplify the required modal integrations, it has been assumed that waveguides a and b have a common symmetry axis.

II. Modal Analysis

The following presentation of the modal analysis used in this effort is taken from Wexler [2]. For the present we neglect the effects of the probes that feed the waveguide and sample the reflected and transmitted signals. We also assume that both sections of waveguide a are matched.

To excite the sample, consider a mode $i = 1$ emanating from an ideal matched source in waveguide a and impinging on waveguide b containing the sample at $z = 0$. The coefficient of this mode is a_1, those for the backscattered modes are $a_2, a_3, \cdots, a_i, \cdots$, and ρa_1 as well, where ρ is the reflection coefficient. Taking $\overline{E}$ to be the total transverse electric-field vector within the aperture at the discontinuity, the field expanded in terms of modes just to the left of junction 1 ($z = 0$) is

$$\overline{E} = (1+\rho)a_1\overline{e}_{a1} + \sum_{i=2}^{\infty} a_i \overline{e}_{ai}\,. \tag{1}$$

Subscript a denotes quantities relative to waveguide a. Similarly, the total magnetic field may be expressed by

$$\overline{H} = (1-\rho)a_1\overline{h}_{a1} + \sum_{i=2}^{\infty} a_i \overline{h}_{ai}\,. \tag{2}$$

Referring again to Fig. 1, we express the aperture fields at $z = 0$ in terms of modes in b. Each transmitted evanescent or propagating mode j reaching junction 2 ($z = \ell$) partially reflects and scatters power into other modes k, some of which return to junction 1. These are accounted for by the scattering coefficients S_{jk}. The total transverse electric and magnetic fields just to the right of junction 1 are given by

$$\overline{E} = \sum_{j=1}^{\infty} b_j \left(\overline{e}_{bj} + \sum_{k=1}^{\infty} S_{jk}\overline{e}_{bk} \right) \tag{3}$$

and

$$\overline{H} = \sum_{j=1}^{\infty} b_j \left(\overline{h}_{bj} - \sum_{k=1}^{\infty} S_{jk}\overline{h}_{bk} \right). \tag{4}$$

Poundary conditions to be satisfied at the discontinuity are as follows: transverse electric and magnetic fields must be continuous across the aperture, and the electric field tangential to the conducting walls must vanish. Following the procedure of Wexler, the following equations result:

For $m \neq 1$,

$$\rho \int_a \overline{e}_{a1} \times \overline{h}_{bn} \cdot \overline{u}_z\, ds - \sum_{j=1}^{N} \frac{b_j}{a_1} \sum_{i=2}^{M} \frac{\int_a \overline{e}_{ai} \times \overline{h}_{bj} \cdot \overline{u}_z\, ds - \sum_{k=1}^{N} S_{jk} \int_a \overline{e}_{ai} \times \overline{h}_{bk} \cdot \overline{u}_z\, ds}{\int_a \overline{e}_{ai} x \overline{h}_{ai} \cdot \overline{u}_z\, ds} \cdot \int_a \overline{e}_{ai} \times \overline{h}_{bn} \cdot \overline{u}_z\, ds - \left(\frac{b_n}{a_1} + \sum_{j=1}^{N} \frac{b_j}{a_1} S_{jn} \right) \int_b \overline{e}_{bn} \times \overline{h}_{bn} \cdot \overline{u}_z\, ds = -\int_a \overline{e}_{a1} \times \overline{h}_{bn} \cdot \overline{u}_z\, ds\,. \tag{5}$$

For $m = 1$,

$$\rho \int_a \overline{e}_{a1} \times \overline{h}_{a1} \cdot \overline{u}_z\, ds + \sum_{j=1}^{N} \frac{b_j}{a_1} \left(\int_a \overline{e}_{a1} \times \overline{h}_{bj} \cdot \overline{u}_z\, ds - \sum_{k=1}^{N} S_{jk} \int_a \overline{e}_{a1} \times \overline{h}_{bk} \cdot \overline{u}_z\, ds \right) = \int_a \overline{e}_{a1} \times \overline{h}_{bn} \cdot \overline{u}_z\, ds \tag{6}$$

$$\frac{a_i}{a_1} = \frac{-\sum_{j=1}^{N} \frac{b_j}{a_1} \left(\int_a \overline{e}_{ai} \times \overline{h}_{bj} \cdot \overline{u}_z\, ds - \sum_{k=1}^{N} S_{jk} \int_a \overline{e}_{ai} \times \overline{h}_{bk} \cdot \overline{u}_z\, ds \right)}{\int_a \overline{e}_{ai} \times \overline{h}_{ai} \cdot \overline{u}_z\, ds}, \tag{7}$$

where $n = 1, 2, \cdots, N$. Equations (5) and (6) form a system of $N+1$ equations in $N+1$ unknowns, b_n and ρ. Equation (7) gives a_i in terms of b_j once they are determined by solution of (5) and (6).

To solve (5)–(7) the scattering matrix S_{jk} may be evaluated using symmetric and antisymmetric excitation since the sample is symmetric about the $z = \ell/2$ plane. Symmetric excitation of the groove is obtained by having two incident fields in waveguide a, one traveling in the $+z$ direction and the other in the $-z$ direction, such that the E fields are in phase in the $z = \ell/2$ plane; antisymmetric excitation is obtained if these fields are 180° out of phase. Under these conditions, $S_{jk} = 0$ for $j \neq k$, and

$$S_{jj} = \pm e^{-\Gamma_j 1}\,. \tag{8}$$

The plus and minus signs in (8) correspond to symmetric and antisymmetric excitation, respectively. To determine the reflection coefficient, or any other modal coefficient on the reflection (incident) side of the sample add the results for symmetric and antisymmetric excitation. The transmission coefficient and all modal coefficients on the transmission side are obtained by subtraction of the corresponding antisymmetric

result from the symmetric result. For example, if we let ρ_s be the reflection coefficient obtained by solving (5) and (6) for symmetric excitation, and ρ_a for antisymmetric, then for the actual excitation of a single incident mode

$$R = \frac{\rho_s + \rho_a}{2} \tag{9}$$

and

$$T = \frac{\rho_s - \rho_a}{2}. \tag{10}$$

III. Waveguide Modes

We now need to define a set of modes to expand the waveguide fields. A suitable set of modes can be found from those given in [3] for the similar problem of a waveguide boundary reduction. The modes in waveguides a are

$$\overline{e}_{ai} = \overline{u}_x \sin\left(\frac{p\pi(2y - t + w)}{2w}\right) \cos\left(\frac{q\pi(2x - h + v)}{2v}\right) \tag{11}$$

and

$$\begin{aligned}\overline{h}_{ai} = {} & \overline{u}_y y_{ai} \sin\left(\frac{p\pi(2y - t + w)}{2w}\right) \cos\left(\frac{q\pi(2x - h + v)}{2v}\right) \\ & - \overline{u}_x \sqrt{-1} \sqrt{\frac{\epsilon}{\mu}\frac{\lambda}{2\pi}} \frac{\frac{pq\pi^2}{wv}}{\sqrt{\left(\frac{p\pi}{w}\right)^2 + \left(\frac{q\pi}{v}\right)^2 - \left(\frac{2\pi}{\lambda}\right)^2}} \\ & \cdot \cos\left(\frac{p\pi(2y - t + w)}{2w}\right) \sin\left(\frac{q\pi(2x - h + v)}{2v}\right),\end{aligned} \tag{12}$$

where u_x and u_y are unit vectors, p and q are the conventional mode numbers, and y_{ai} is the wave admittance of the ith mode given by

$$y_{ai} = \sqrt{-1} \sqrt{\frac{\epsilon}{\mu}\frac{\lambda}{2\pi}} \frac{\left(\frac{2\pi}{\lambda}\right)^2 - \left(\frac{p\pi}{w}\right)^2}{\sqrt{\left(\frac{p\pi}{w}\right)^2 + \left(\frac{q\pi}{v}\right)^2 - \left(\frac{2\pi}{\lambda}\right)^2}}. \tag{13}$$

In region b, the transverse components of the modes are complicated somewhat by allowing for limited anisotropic characteristics. If the tensors are diagonal, with $\epsilon_x = \epsilon_z$ and $\mu_x = \mu_z$, we have

$$e_{bj} = \overline{u}_x \sin\left(\frac{r\pi y}{t}\right) \cos\left(\frac{s\pi x}{h}\right) \tag{14}$$

and

$$\begin{aligned}h_{bj} = {} & \overline{u}_y y_{bj} \sin\left(\frac{r\pi y}{t}\right) \cos\left(\frac{s\pi x}{h}\right) \\ & - u_x \frac{\sqrt{-1}}{\omega\mu_x\Gamma_j} \frac{rs\pi^2}{th} \cos\left(\frac{r\pi y}{t}\right) \sin\left(\frac{s\pi x}{h}\right),\end{aligned} \tag{15}$$

where r and s are the mode numbers, and y_{bj} is given by

$$y_{bj} = \frac{\sqrt{-1}}{\omega\mu_z} \frac{\omega^2\mu_z\epsilon_z - \left(\frac{r\pi}{t}\right)^2}{\Gamma_j}, \tag{16}$$

where Γ_j is the propagation constant for mode j in guide b and is given by

$$\Gamma_j = \sqrt{\left(\frac{s\pi}{h}\right)^2 + \frac{\mu_y}{\mu_z}\left(\frac{r\pi}{t}\right)^2 - \omega^2\mu_y\epsilon_z}. \tag{17}$$

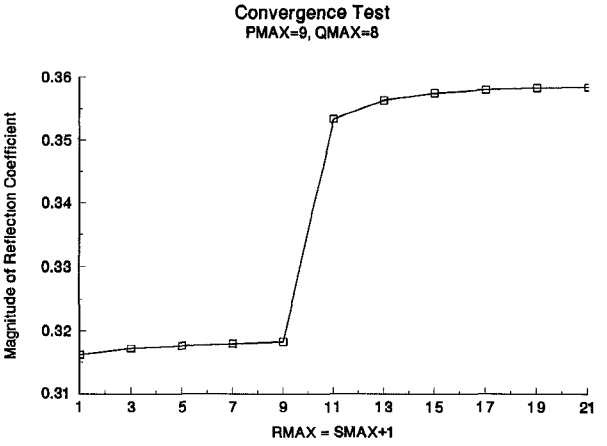

Fig. 2. Effect of the number of modes used to describe the fields in waveguide b on the computed value of the reflection coefficient.

The modes in guide b are TE to y. Modes are numbered consecutively, that is, $i = 1, 2, 3, \cdots$, and $j = 1, 2, 3 \cdots$, where each value of i corresponds to particular values for p and q, etc. Due to symmetry, not all modes are excited; p and r are always odd, and q and s are even (or 0) for this geometry and for an incident TE_{10} mode in guide a.

The integrations needed to evaluate the terms in (5)–(7) are fairly straightforward for this problem, and are given in [3].

IV. Convergence of the Modal Analysis

When using the modal analysis method, care must be taken in choosing the number of modes used to expand the fields in the two different waveguide regions. This has been discussed in the literature [4], [5], with the basic rule being that more modes are required in the larger waveguide than in the smaller.

To illustrate the convergence phenomenon for this geometry, results for the magnitude of the reflection coefficient as a function of the number of modes used are presented in Fig. 2 and 3. The relative complex permittivity of the sample was $27.0 - j4.0$, and relative complex permeability was $5.2 - j0.8$. The dimensions of waveguide a were held constant at $w = 45.7$ cm and $v = 22.9$ cm. These dimensions result in a dominant mode cutoff frequency of 328 MHz. Waveguide b has dimensions $t = 47.6$ cm and $h = 24.8$ cm for a groove depth of 0.95 cm. All calculations are at 500 MHz, approximately in the middle of the waveguide single mode frequency band. The sample thickness ℓ is 2.54 cm.

To facilitate plotting the results, we introduce the variables PMAX, QMAX, RMAX, and SMAX. These are the maximum values of p, q, r, and s, the modal numbers in the a (p, q) and b (r, s) waveguides, respectively. These are defined by the modes sets given previously.

For the first convergence results, shown in Fig. 2, PMAX and QMAX were held at 9 and 8, respectively, whereas RMAX and SMAX were increased simultaneously. This figure clearly illustrates the phenomenon known as "relative convergence" [5]. The unwary practitioner may perform a convergence test by increasing the number of modes in waveguide b, observe a small change in the reflection coefficient as the maximum mode coefficients PMAX and QMAX are being increased, and

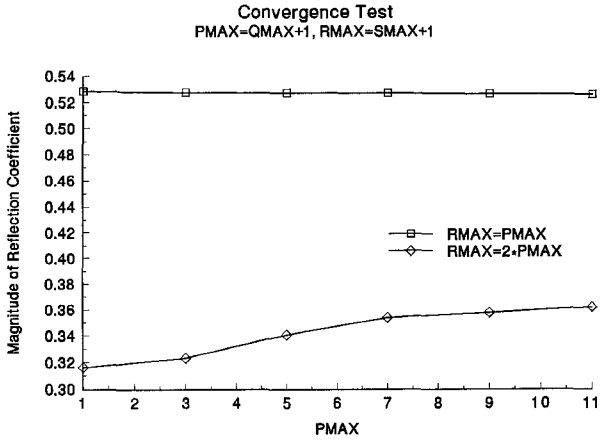

Fig. 3. Effect of varying the number of modes used to expand the waveguide fields. The maximum value of the modal coefficients in b is kept equal to and twice that of a.

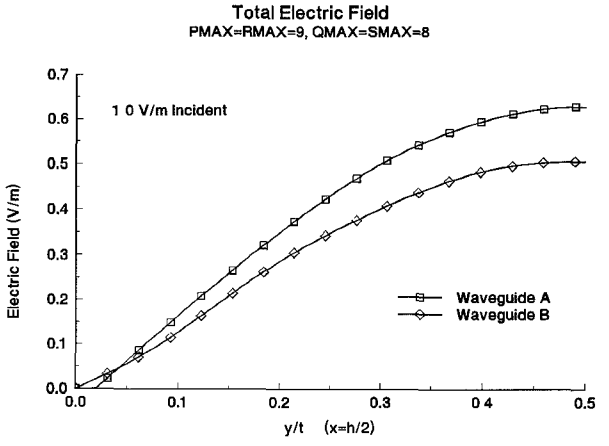

Fig. 4. Electric field across the waveguide junction at $z = \ell$ computed with equal maximum modal coefficients in the two waveguides.

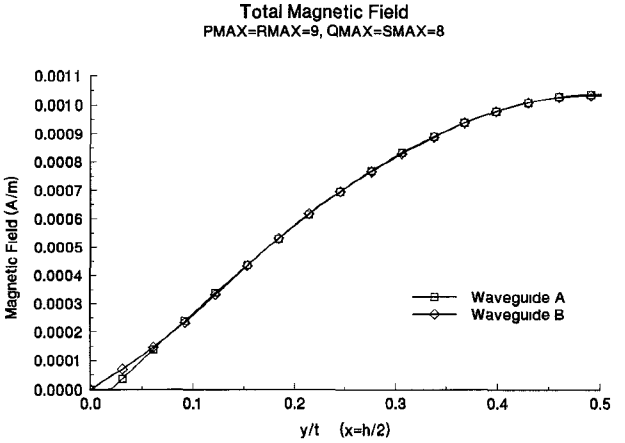

Fig. 5. Magnetic field across the waveguide junction at $z = \ell$ computed with equal maximum modal coefficients in the two waveguides.

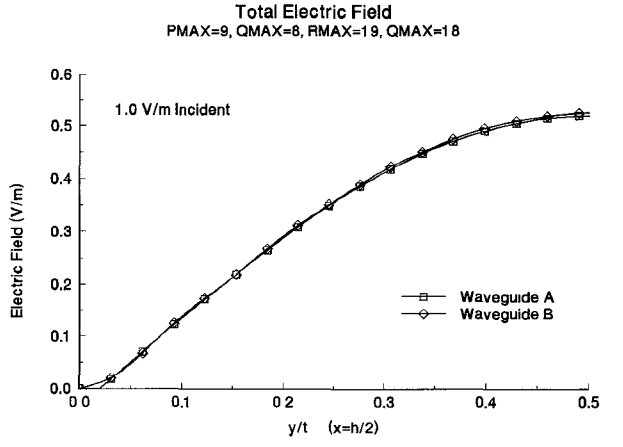

Fig. 6. Electric field across the waveguide junction at $z = \ell$ computed with the maximum modal coefficients in waveguide b twice those in waveguide a.

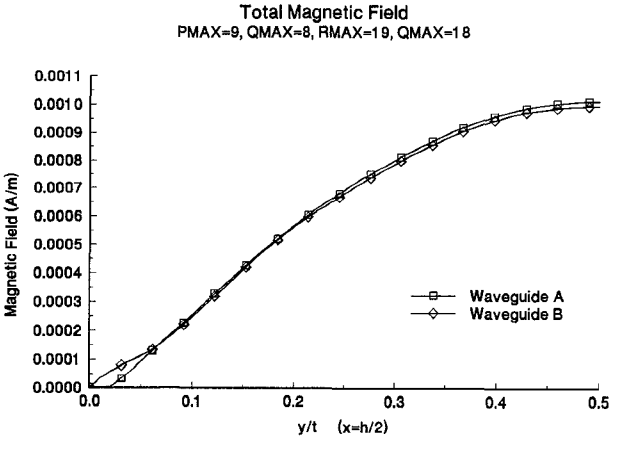

Fig. 7. Magnetic field across the waveguide junction at $z = \ell$ computed with the maximum modal coefficients in waveguide b twice those in waveguide a.

stop at RMAX = 9, SMAX = 8, never (or more likely too late) realizing that the method has not converged to a correct value. The reasons for this are explained in [4] and [5], and we observe a rapid convergence to a stable reflection coefficient value once RMAX and SMAX are allowed to exceed PMAX and QMAX.

For a different look at the convergence phenomenon, consider the results in Fig. 3 where the maximum modal coefficients in waveguide a are increased, and the corresponding maximums in waveguide b are increased simultaneously, being either kept equal to or twice the number as in waveguide a. Looking at Fig. 3 one would not conclude that the results with RMAX and SMAX at twice their corresponding values in waveguide a are more accurate.

To form a conclusion, let us consider examining the accuracy of the field match at the waveguide junctions for two cases, one with PMAX = RMAX = 9 and QMAX = SMAX = 8, and the other with PMAX = 9 and QMAX = 8 but with RMAX = 19 and SMAX = 18. These results, in Figs. 4–7, clearly show the improved accuracy in the field match with the greater number of modes in the larger waveguide.

Figs. 4 and 5 show that without an adequate number of modes in the larger waveguide the magnetic fields in the aperture plane match exactly, since they are determined entirely by the incident mode field, but the electric fields are a very poor match. Figs. 6 and 7 show the fields at the discontinuity with the maximum modal coefficients in waveguide b twice those in a. Once the number of modes in waveguide b is increased, the magnetic field match is not quite as good as before, since

the magnetic fields in waveguide b are no longer determined entirely by the incident field but are attempting to match the surface current on the conducting wall, but the electric field match is now greatly improved. A more detailed discussion of this phenomenon is given in [4].

V. Determining the Sample Constitutive Parameters

The modal analysis method allows us to calculate the electromagnetic fields at any point inside the waveguide region. However, the goal is to assess the effects of the waveguide groove and sample probe locations on the accuracy of the measurement of the constitutive parameters of the sample material in waveguide b. To do this we must develop a means to convert our modal analysis field calculations to simulated measured results of the complex permittivity and permeability of the sample material.

Our approach is to simulate the measurement process of converting measured values of the reflection and transmission coefficients to the complex permittivity and permeability of the sample in waveguide b. Using this result, the modal analysis is used to compute the reflected and transmitted electric fields at the sample probe locations. Then these simulated reflection and transmission coefficients, which include the effects of the wall groove and the resulting higher order modes, are used to calculate the constitutive parameters of the material in waveguide b, as would be done if the same reflection and transmission coefficients had been measured.

To derive a relationship between the (computer-simulated) measured values of the complex reflection and transmission coefficients, R and T, and complex μ and ϵ, we define z_a and z_b as the dominant propagating modal impedances in waveguides a and b, and Γ_a and Γ_b as the corresponding propagation constants given earlier. To simplify our calculations, we assume isotropic sample material. Using transmission line methods, we find

$$z_b \coth(\Gamma_b \ell/2) = z_a(1+\rho_s)/(1-\rho_s) \tag{18}$$

and

$$z_b \tanh(\Gamma_b \ell/2) = z_a(1+\rho_a)/(1-\rho_a)\,. \tag{19}$$

Dividing (17) by (18) and solving for Γ_b we obtain

$$\Gamma_b = (2/\ell)\tanh^{-1}\left[\left(\frac{1+\rho_a}{1-\rho_a}\cdot\frac{1-\rho_s}{1+\rho_s}\right)^{1/2}\right] \tag{20}$$

from which we can easily obtain z_b from application of (18) or (19).

Assuming a TE_{10} mode ($p=1, q=0$), with $z_b = 1/y_b$, solving (16) and (17), we find that in waveguide b

$$\mu = -\frac{j}{\omega}\Gamma_b z_b\,. \tag{21}$$

Having determined μ from (21), we use (17) to find the complex permittivity ϵ of the sample.

Thus we have derived an approach to determine complex μ and ϵ from modal analysis calculations which can include effects of wall grooves and sample probe location. We use this in the next section to predict the errors that might be expected when using this waveguide geometry to measure μ and ϵ.

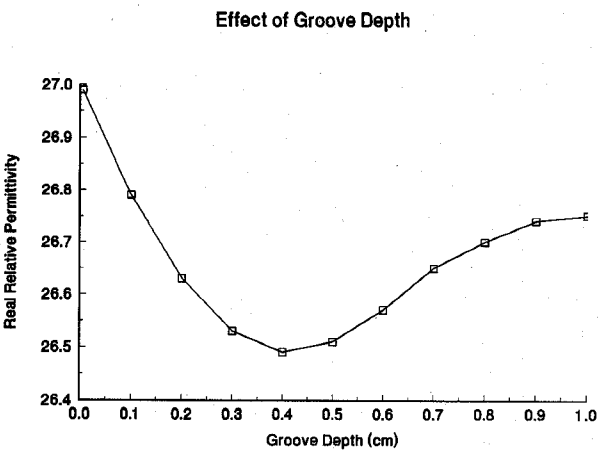

Fig. 8. Mode matching prediction of measured value of the real part of the sample permittivity versus groove depth. Actual value is 27.

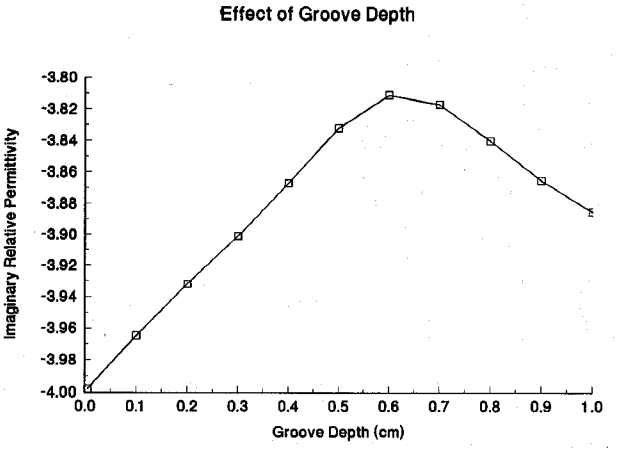

Fig. 9. Mode matching prediction of measured value of the imaginary part of the sample permittivity versus groove depth. Actual value is -4.

VI. Sample Results

Since the modal analysis implementation is so general, it would not be reasonable to try to present an exhaustive study of the errors that might be predicted. To illustrate its capabilities, a particular geometry and material have been chosen for demonstration purposes.

The relative complex permittivity of the sample was again set at $27.0 - j4.0$, and relative complex permeability was $5.2 - j0.8$. The sample thickness ℓ was decreased to 0.635 cm (1/4 in). The dimensions of waveguide a were held constant at $w = 45.7$ cm and $v = 22.9$ cm. All calculations are at 500 MHz. Note that, for these dimensions, it would be quite difficult to hold the sample in place using a conventional sample holder.

For this example, the waveguide groove depth, $(t - w)/2$ and $(h - v)/2$ in Fig. 1, has been varied from 0 to 1 cm, whereas the distance from the material faces at $z = 0$ and $z = \ell$ to the sample probes was held constant at 20 cm. The electric fields computed at the center of the waveguide at the probe distances were used to compute simulated reflection and transmission coefficients, and the complex constitutive parameters were then

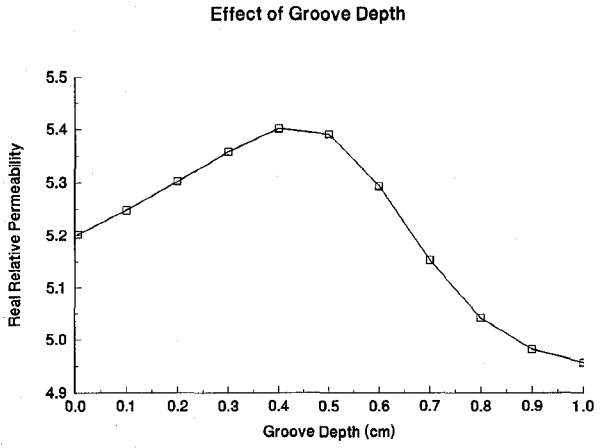

Fig. 10. Mode matching prediction of measured value of the real part of the sample permeability versus groove depth. Actual value is 5.2.

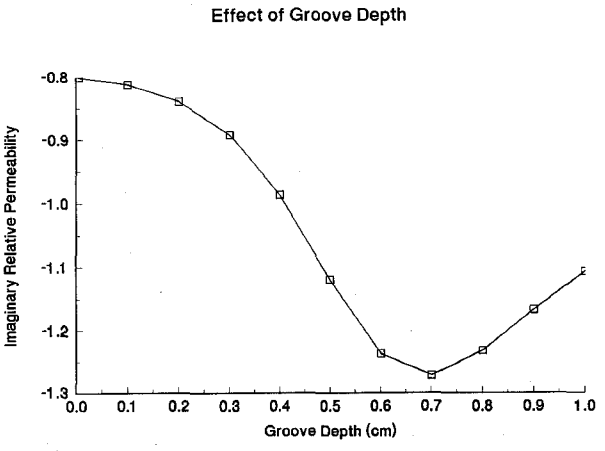

Fig. 11. Mode matching prediction of measured value of the imaginary part of the sample permeability versus groove depth. Actual value is -0.8.

determined as described earlier. For these results, PMAX = 9, QMAX = 8, RMAX = 19, and SMAX = 18.

Figs. 8–11 show the mode matching estimates of the measured values of the complex constitutive parameters as a function of the groove depth. As expected, for a groove depth of zero ($w = t$ and $v = h$), the measured values agree almost exactly with those specified. As the groove depth is increased, the simulated measured values deviate from those specified.

VII. Conclusions

The preceding results illustrate that the modal analysis method can be very useful in assessing the potential error, which may be a result of holding samples in place using grooved waveguide walls. This capability should be very useful is designing and evaluating waveguide measurements of thin samples of lossy materials.

Acknowledgment

Dr. D. Levine defined the problem, provided helpful discussions during the solution, and edited the manuscript.

References

[1] S. B. Wilson, "Modal analysis of the gap effect in waveguide dielectric measurements," *IEEE Trans. Microwave Theory Tech.*, vol. MTT-36, no. 4, pp. 752–756, Apr. 1988.

[2] A. Wexler, "Solution of waveguide discontinuities by modal analysis," *IEEE Trans. Microwave Theory Tech.*, vol. MTT-15, pp. 508–517, Sept. 1967.

[3] R. Luebbers, "Analysis of thick rectangular waveguide windows with finite conductivity," *IEEE Trans. Microwave Theory Tech.*, vol. MTT-21, pp. 461–468, July 1973.

[4] P. H. Masterman *et al.*, "Computer field-matching solution of waveguide transverse discontinuities," *Proc. IEE*, vol. 118, pp. 51–63, Jan. 1971.

[5] S. W. Lee *et al.*, "Convergence of numerical solutions of iris-type discontinuity problems," *IEEE Trans. Microwave Theory Tech.*, vol. MTT-19, pp. 528–536, June 1971.

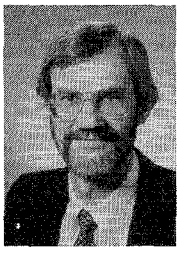

Raymond Luebbers received the B.S.E.E. degree from the University of Cincinnati, and the M.S.E.E. and Ph.D. degrees from Ohio State University, where he was a member of the ElectroScience Laboratory.

He has been an electrical engineering faculty member at Ohio University, and a research scientist at the Lockheed–Palo Alto research laboratory. He was also a Visiting Professor at Tohoku University, Sendai, under the National Science Foundation program for U.S./Japan Cooperative Research. He is currently Professor of Electrical Engineering at The Pennsylvania State University. Dr. Luebbers has written series of technical papers in several areas, including frequency selective surfaces, geometrical theory of diffraction, and FDTD.

He is a Senior Member of the Antennas and Propagation Society of the IEEE, and is on the Board of Directors of the Applied Computational Electromagnetics Society. He has chaired a number of IEEE and URSI conference sessions, including an URSI General Assembly session, and reviews articles for several technical journals.